Investigation of Late-Cycle Soot Oxidation Using Laser Extinction and In-Cylinder Gas Sampling at Varying Inlet Oxygen Concentrations in Diesel Engines

Yann Gallo[a], Ville Berg[b], Johan Simonsson[c], Erik Svensson[a], MengQin Shen[a], Per-Erik Bengtsson[c], Joakim Pagels[b], Martin Tunér[a], Antonio Garcia[d], Öivind Andersson[a]

[a] Division of Combustion Engines, Lund University, Sweden

[b] Division of Ergonomics and Aerosol Technology, Lund University, Sweden

[c] Division of Combustion Physics, Lund University, Sweden

[d] CMT Motores Térmicos, Universitat Politécnica de Valencia, Spain

Abstract

This study focuses on the relative importance of O_2 and OH as oxidizers of soot during the late cycle in diesel engines. Laser-extinction measurements of soot oxidation rates are made in an optically accessible engine. These are combined with in-cylinder gas sampling data from a single-cylinder engine fitted with a fast gas sampling valve. Both measurements confirm that the in-cylinder soot oxidation slows down when the inlet concentration of O_2 is reduced. A 50% decrease in intake O_2 concentration reduces the soot oxidation rate by 600%, a discrepancy indicating that O_2 in itself is not the main soot oxidizing species. Chemical kinetics simulations of OH concentrations in the oxidation zone and estimates of the OH-soot oxidation rate point towards OH being the dominant oxidizer.

Introduction

Diesel engines are favored by high efficiencies but are challenged by high emissions of nitrous oxides (NO_x) and particulate matter (PM), if not coupled with adequate exhaust aftertreatment technologies such as NO_x adsorbers and diesel particulate filters (DPF). Diluting the charge by Exhaust Gas Recirculation (EGR) is a widespread method for reducing the NO_x emissions by decreasing the combustion temperature. On the other hand, EGR

generally increases PM emissions due to deteriorating in-cylinder soot oxidation rates [1,2]. Previous studies indicate that, under most conditions applicable to diesel engines, this oxidation has a dominating influence on the soot emission levels [2-4].

EGR reduces the intake oxygen concentration. This has a number of potential effects on the soot oxidation process. First, it will decrease the availability of oxygen during the late cycle, which could limit the oxidation rate. It also lowers the flame temperature, slowing the chemical kinetics of the oxidation process as well as decreasing the formation of hydroxyl radicals (OH) [5], which is believed to be the main oxidizing species [6-10].

The purpose of this study to cast light on the relative importance of O_2 and OH as soot oxidizers during the late cycle. It is based on data from optical measurements and in-cylinder gas sampling. The optical measurements are made using laser extinction in an optically accessible single-cylinder engine fitted with a Bowditch-type piston extender [11]. The gas sampling data are acquired from a single-cylinder engine without optical access, fitted with a fast gas sampling valve. The analysis is complemented with a simulation of OH availability in the flame using a zero-dimensional (0-D) reactor model.

Experimental facilities

Engine Setup

The engine used for the optical study is a heavy-duty direct-injection diesel engine based on a Scania D12, operated as a single-cylinder engine. A single-cylinder version of a Scania D13 is used for the in-cylinder gas sampling measurements. These engines are henceforth referred to as the optical and the all-metal engine. In order to produce as similar conditions as possible, both configurations employ the same cylinder head and the same injector. A Scania XPI

common-rail fuel injection system capable of fuel pressures up to 2500 bar is used. The injector is a stock item with eight nozzle holes. The fuel used is Swedish MK1 diesel. Specifications of the engines, fuel system and fuel are given in Table 1.

Table 1.

Engine and fuel specifications

Engine base type	Scania D12 DI diesel	Scania D13 DI diesel
Bore	127 mm	130 mm
Stroke	154 mm	160 mm
Comp. Ratio	15.6	16
Swirl	1.6	
Displacement	1.95 l	2.12 l
EGR	External	Internal
Injection system	XPI common rail	
Nozzle flow number	207 pph	
Number of holes	8	
Firedeck angle	17 °	
Hole diameter	0.175 mm	
Fuel type	MK1 Diesel	
Cetane number	51	
Density	815 kg/m^3	
Lower Heating Value	42.9 MJ/kg	
C/H	0.53	

The two setups use different sources of EGR. On the optical engine, exhaust gases are produced using a diesel furnace operating at stoichiometric conditions. These are mixed with fresh air, heated and compressed to the desired inlet conditions in order to achieve a stable external source of "EGR". On the all-metal engine, exhaust gases are taken from the exhaust manifold and fed to the intake manifold, using flow and back-pressure valves to control the flow. The intake O_2 concentration is used to measure the EGR rate. In the optical engine, it is measured during engine operation without injection by a lambda sensor located in the exhaust. For the all-metal engine, the concentration of inlet O_2 is calculated as:

$$O_{2,in} = \frac{CO_{2,in}}{CO_{2,ex}}\left(O_{2,ex} - O_{2,amb}\right) + O_{2,amb} \quad (1)$$

where $O_{2,ex}$ is the exhaust O_2 concentration measured by a lambda sensor, $O_{2,amb}$ is the ambient O_2 concentration set at 20.95%. $CO_{2,in}$ and $CO_{2,ex}$ are the CO_2 concentrations of inlet and exhaust both measured using an infrared detector in an AVL AMA i60 emission system.

Another difference between the setups is the shape of the piston bowl. In the D12 engine, the bottom of the bowl is flat in order to facilitate the optical access, while the D13 engine has a slightly conical bowl bottom. As shown in Figure 1, both configurations had open combustion chambers. While the differences should give rise to some differences in the gas motion, the overall trends in the oxidation process are expected to be highly comparable between the engines.

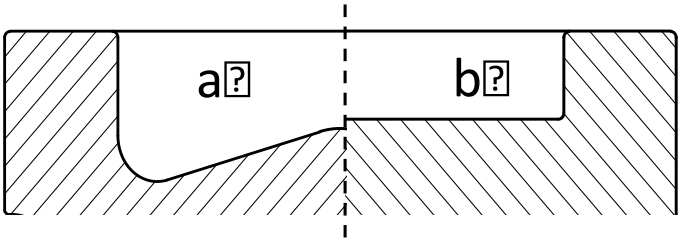

Figure 1.

Profile of the metal piston used in the D13 engine (a) and of the quartz piston used in the D12 engine (b).

Operating conditions

The engines are operated at a speed of 1200 rpm and a load of 6 bar $IMEP_g$. The EGR rate is varied in order to obtain various inlet O_2 concentrations (13%, 15% and 21%). The cylinder pressure is monitored using a side-mounted Kistler 6125C transducer coupled to a Kistler 5011B10 charge amplifier. A crank angle encoder giving 1800 pulses per revolution is used, resulting in one pulse per 0.2 CAD. The injection pressure is kept constant as well as the

duration of injection (650 µs). The start of injection is adjusted in order to maintain CA50 at approximately 9 CAD ATDC. A summary of the operating conditions is given in Table 2.

Table 2.

Engines operating conditions

Operating conditions		
Engine	Scania D12 DI diesel	Scania D13 DI diesel
Speed	1200 rpm	
Load	6 bar IMEPg	
Pinj	2000	
CA50	8 CAD ATDC	
SOI	Adjusted to keep CA50 constant	
DOI	650µs	
Inlet P	1.8 bar	1.65 bar
Inlet T	70°C	
Fuel	MK1 Swedish Diesel	
EGR rate	Variable (13% to 21% O_2)	

In order to compensate for the difference in compression ratio, the top dead center (TDC) conditions in temperature and density are matched between the engines. This is realized by applying adiabatic compression calculations, leading to the use of a substantially lower inlet pressure on the all-metal engine. A sample motored pressure trace at 15% inlet O_2 from the optical engine is compared with a motored one from the all-metal engine without EGR in Figure 2a. The apparent heat release rate (AHRR) from a case with combustion at 15% O_2 is shown in Figure 2b for the two engines. The differences in thermodynamic conditions at TDC and during combustion are minor, justifying the validity of the comparison between setups.

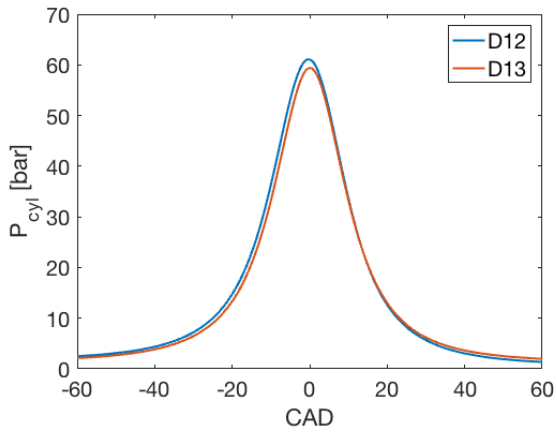

Figure 2a.

Sample motored trace for the 15% [O_2] case. The D13 trace (all-metal engine) is recorded without EGR.

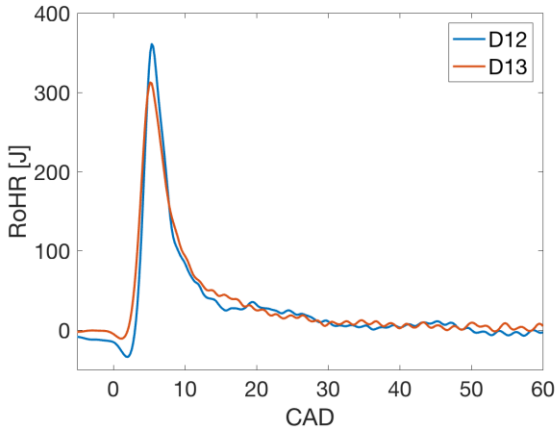

Figure 2b.

Sample AHRR for the 15% [O_2] case.

Soot measurement techniques

Laser extinction method

The laser extinction technique is a quantitative measurement technique for soot that has been applied successfully in combustion engines for several decades [2,3, 12-14] as well as in spray vessels [15-17]. The intensity of a laser beam decreases as it passes an absorbing medium, *e.g.* containing soot. The initial and transmitted intensities, I_0 and I, are measured

and, assuming that the in-cylinder combustion medium is optically thin, the Beer-Lambert law applies:

$$I = I_0 e^{-KL} \tag{2}$$

Here, K is the extinction coefficient and L is the length of the absorbing medium, in this case the vertical extent of the combustion chamber. Extinction is any process that decreases the initial laser intensity, and is thus a combination of absorption and scattering of light out of the beam path. In the Rayleigh limit, where the particle sizes are much smaller than the laser wavelength, the scattering is assumed to be negligible and K is then the absorption coefficient [18]. Under this assumption, K can be related to the soot volume fraction, f_v, as

$$K = \frac{f_v 6\pi E(m)}{\lambda}, \tag{3}$$

where λ is the laser wavelength. $E(m)$ is the refractive index function, representing the imaginary part of $(m^2\text{-}1)/(m^2\text{+}2)$, where m is the complex refractive index of the soot particles, see *e.g.* [19]. Throughout this paper, the soot concentration is represented by the product KL, which is directly related to the average soot concentration in the beam path and obtained directly from the relative transmission measurement. This product thus remains constant if the soot content in the beam path remains constant, even if the piston moves. A decrease in KL after the end of injection (EOI) can thereby be attributed to net oxidation of the soot in the cylinder.

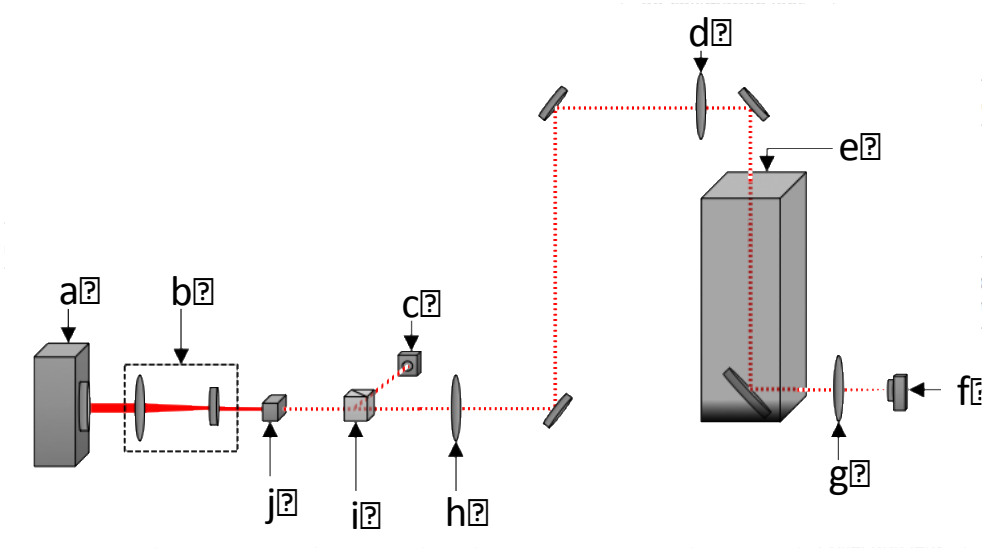

Figure 3.

The parts of the laser extinction setup. Diode laser (a), telescope lenses (b), photodiode for the reference signal (c), re-collimation lens (d), engine (e), photodiode (f), collection lens (g), re-collimation lens (h), beamsplitter (i), and acousto-optic modulator, or AOM (j).

A schematic representation of the setup is shown in Figure 3. The Bowditch piston extension has a full quartz piston top and a 45° mirror in a fixed position below it. An insert containing an angled window is used in place of one of the exhaust valves, providing optical access from the top of the cylinder. The angle of the window compensates for the angle of the insert and makes it possible to obtain a vertical beam path through the cylinder. A cross-section of this optical access is given in Figure 4. The absence of one exhaust valve does not substantially affect the combustion process since the engine is running at a relatively low speed of 1200 rpm, allowing for effective gas scavenging. A more detailed presentation of the setup can be found in [2].

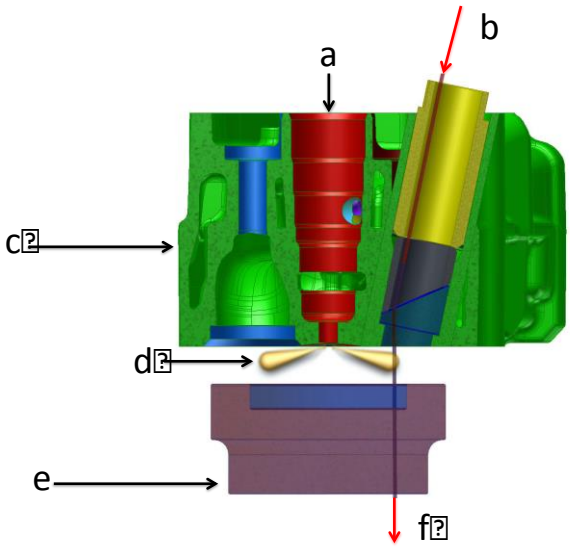

Figure 4.

Section through the cylinder head used in the extinction setup. Injector location (a), laser entrance (b), cylinderhead (c), burning sprays (d), optical piston (e), and laser exit (f).

In-cylinder gas sampling

In-cylinder gas sampling was performed on the all-metal engine, fitted with the same cylinder head as used in the optical measurements. In the all-metal engine, the quartz window in the insert (yellow detail in Figure 4) was replaced with a fast-acting gas sampling valve [20]. During operation, a solenoid hammer actuates the valve by hitting the top of the valve stem, rendering the start of sampling and the sampled flow rate controllable. The valve driver is controlled by a TTM signal from a computer program and triggered on crank angle basis. With these features the gas flow through the valve can be controlled in a wide range, with respect to sampling timing, sampling rate, etc. In this study, the gas flow was kept constant at 1 liter per minute (at ambient atmospheric pressure and temperature) for each sampling point. This volume corresponds to approximately 0.05% of the total cylinder volume. With this flow rate, the minimum step-by-step resolution for the sampling timing can be less than 3.5 crank angle degrees CAD at high in-cylinder pressures [21].

Figure 5 presents the dilution and gas analyzing system. The gases are diluted with nitrogen (N_2) during the first step (D1) in order to prevent further oxidation of the particles. The following steps (D2 and D3) reduce the amount of particles to a level suitable for the aethalometer (Magee Scientific AE33), which measures the Black Carbon (BC) concentration. BC is the part of the particle matter that effectively absorbs light, *i.e.* the soot. The latter is used for on-line chemical particle analysis [22].

The aethalometer is based on the absorption of laser light by the probed particles. Seven different wavelengths are used, ranging from 370 nm to 950 nm. These allow determination of the optical properties of the soot particles. In this study, the BC concentration is obtained as the average of the measurements at the two highest wavelengths (880 nm and 950 nm) in order to reduce interferences from organics or polycyclic aromatic hydrocarbons (PAHs) that absorb in and near the ultraviolet region [20].

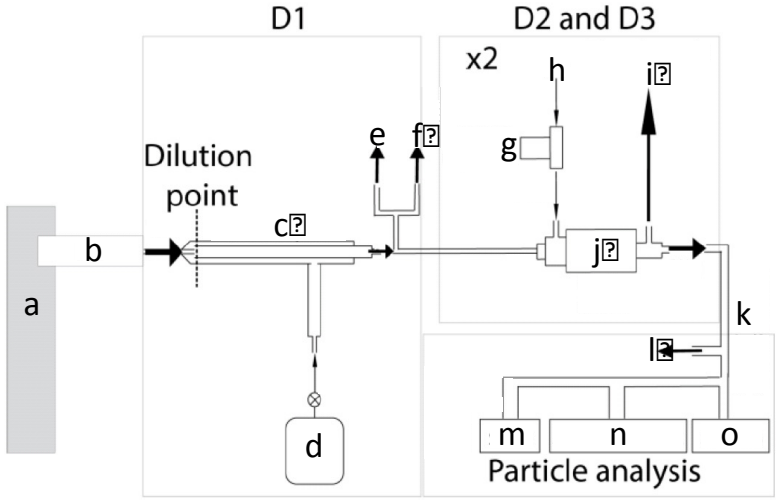

Figure 5.

Diagram of dilution and gas analyzing system [20]. D1, D2 and D3 are dilution steps. Engine (a), fast sampling valve (b), dilution probe (c), N_2 bottle (d), NO_x/CO (e), flow reading (f),

pressure regulator (g), air (h), diluted sample (i, not used), ejector diluter (j), diluted sample (k), NO_x/CO (l), SMPS (m, not used in this article), aethalometer (n). and SP-AMS (o, not used in this study).

Simulation tools

The availability of OH in the flame is evaluated using a *Φ-T* map, a concept first introduced by Kamimoto et al [23]. The *Φ-T* map of OH mass fraction is constructed using a 0-D reactor, from LOGEsoft [24], with constant pressure, temperature and equivalence ratio. The MK1 Diesel was modeled by a surrogate fuel with 70 percent *n*-heptane together with 30 percent toluene. Lars Seidel's chemical mechanism for *n*-heptane could then be applied in the simulations [25]. The addition of toluene is used to mimic the sooting behavior of diesel, which *n*-heptane alone cannot. Such surrogate for diesel fuel has been commonly used in diesel combustion studies [26,27] and ascertained in [28]. The map consists of a grid of nodes at different *Φ* and *T* conditions (the pressure is constant for all nodes). One simulation is performed at every node and the *Φ-T* map shows the OH yield after 2 milliseconds.

Dependency of the soot oxidation rate on O_2 and OH availability

Gallo et al. observed a constant degradation of the soot oxidation rate with reduced intake O_2 level, leading to increased soot emissions [2]. This was accompanied with an increase in the engine-out emissions of soot. Figure 6a shows the optical density, *KL*, in the cylinder for three intake O_2 levels. As previously mentioned, *KL* is proportional to the soot volume fraction in the beam path. The curves show a marked late-cycle decay due to soot oxidation. Figure 6b shows aethalometer data from the all-metal engine. The curves represent the content of BC in samples drawn from the cylinder at different crank angle positions during the cycle. In both these figures it can be seen that the 21% O_2 data set represents the steepest

decay and the 13% O_2 case the slowest. The two measurement setups independently show that a global effect of the reduction in inlet O_2 concentration is a reduction in the rate of soot oxidation.

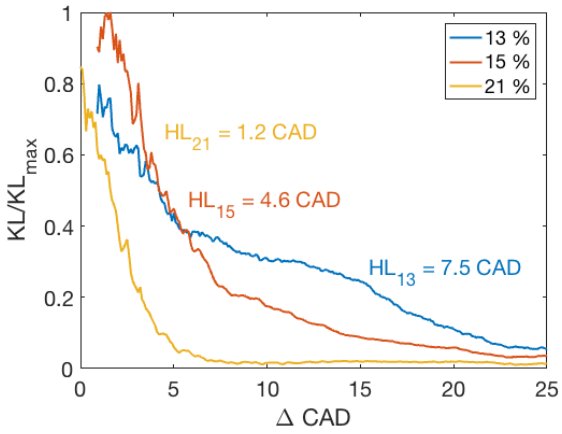

Figure 6a.

Evolution of KL (relative to the peak KL at 15% O_2) in the optical measurements shown from the start of decay. The half-life extracted from the exponential approximation is shown in CAD.

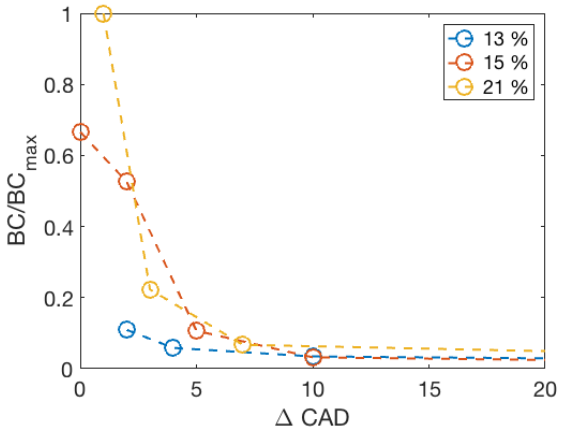

Figure 6b.

Evolution of BC from the in-cylinder sampling measurements shown from the start of decay.

There are several potential ways to quantify these soot oxidation rates. One method is to fit an exponential decay function to the extinction curves and extracting the half-life (HL) [2].

Although the 13% O_2-case in Figure 6a is not perfectly described by an exponential (13% O_2), the half-lives extracted from the curves still give a useful estimate of the overall oxidation rates. When decreasing the O_2 concentration from 21% to 13%, *i.e.* by a factor of less than two, the decay rates in Figure 6a display a six-fold increase. This indicates that the availability of O_2 in itself is not governing the oxidation rate.

O_2 and OH are both important soot oxidizers [8]. According to Bartok and Sarofim [6], both OH and O_2 play a role under lean conditions while OH is likely to be dominating under fuel-rich and stoichiometric conditions [6]. Since the late-cycle soot oxidation is a mixing-controlled combustion process, it is expected to take place near stoichiometric conditions, and OH is thereby expected to be the main soot oxidizer under diesel conditions. About 10–20% of all OH collisions with soot are effective at gasifying a carbon atom [7,10]. Moreover, Guo et al. have shown that soot oxidation by OH has negligible activation energy and they point out that, for premixed and diffusion flames, optimized models indicate that soot oxidation by OH dominates over O_2 [10].

While dilution with EGR affects the availability of O_2, it has an even greater impact on the flame temperature. The flame temperature, in turn, has a strong effect on the availability of OH. Figure 7 represents Φ-T maps obtained using the 0-D reactor model. The colored iso-fields represent the OH concentration and the white, green and red curves represent the adiabatic flame temperatures at the different O_2 concentrations using an initial temperature of 900 K. The maximum adiabatic flame temperature is 2744 K at 21% O_2, and drops to 2196 K for the 15% O_2 case.

Figure 8 shows normalized number densities of OH extracted from Figure 7, plotted against the soot oxidation half-lives displayed in Figure 6a. Since the soot oxidation is expected to occur at stoichiometric conditions, the OH mass fractions are extracted at the maximum flame temperature. As expected, the oxidation rate increases with the OH concentration in the flame. It can be noted that the six-fold decrease in half-life previously mentioned is accompanied by a roughly six-fold increase in OH availability.

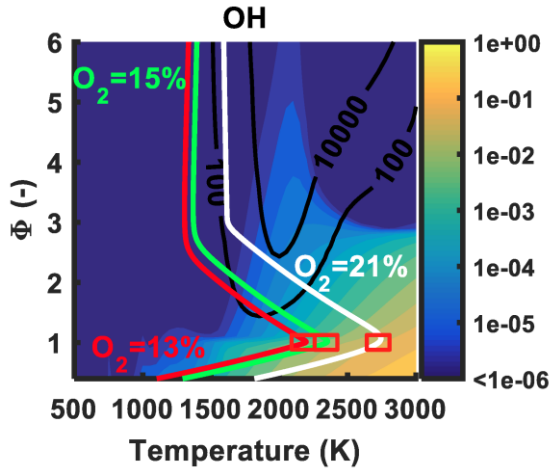

Figure 7.

Φ-T map of OH mass fraction constructed using a 0-D reactor with constant pressure, temperature and equivalence ratio. The three red squares highlight the maximum adiabatic flame temperature corresponding to the three cases (13, 15 and 21% O_2). The scale on the right represents the mass fraction of OH species.

Besides the availability of OH, the local temperature could be expected to affect the soot oxidation rate. In Seidel's mechanism, however, the activation energy for OH-soot reactions is zero, yielding a dependence on OH concentration and the soot area-to-volume ratio, but not on temperature. This is motivated by OH being a very reactive species. The current study provides no data on soot morphology but, assuming that the area-to-volume ratio remains

constant, the temperature dependence of the OH-soot reactions can be estimated using the model of Neoh et al. [29]

$$\omega_{OH} = \gamma_{OH} \frac{3 n_{OH}}{N_A} \left(\frac{8RT}{\pi M_{OH}} \right)^{1/2}. \quad (4)$$

Here, ω_{OH} is the soot oxidation rate, n_{OH} and M_{OH} are the number density and the molar mass of OH, R is the general gas constant and N_A is Avogadro's number. γ_{OH} is the collisional frequency between OH and the soot surface and is assigned a value of 0.13 by Neoh *et al.* [29]. Inserting the OH concentrations and the peak adiabatic flame temperatures from the simulations into this model yields the oxidation rates presented in Figure 8 alongside the OH number density. Both the number densities and the rates are normalized to facilitate comparison. Although the temperature drops by 25%, the estimated oxidation rate drops at the same rate as the OH concentration. This supports both the assumption that the OH-soot reactions are not temperature dependent, and the claim that OH is the dominant soot oxidizer.

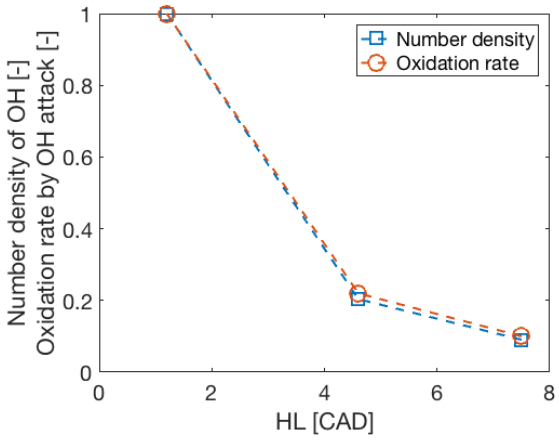

Figure 8.

Variation of the relative number density of OH (blue curve) and soot oxidation rate according to Neoh et al. [32] (red curve) at the 3 cases studied, versus the variation of the oxidation half-life.

Conclusions

The in-cylinder soot oxidation slows down when the inlet concentration of O_2 is reduced. This observation has been confirmed through measurements using two techniques on two different engine setups. Decreasing the intake O_2 concentration by 50% reduces the soot oxidation rate by 600%. The discrepancy between these numbers indicates that O_2 in itself is not the main soot oxidizing species.

The reduction of inlet O_2 concentration has a strong impact on the adiabatic flame temperature, and thereby on the mass fraction of OH during combustion. When the maximum flame temperature drops from 2700 K to 2400 K, the OH concentration drops roughly six times. This corresponds well to the drop in the oxidation rate. Both the chemical mechanism used for the OH simulations and the soot oxidation model by Neoh *et al.* state that the temperature dependence of the OH-soot oxidation reactions is negligible, due to the high reactivity of OH radicals. In combination, these findings indicate that OH is the dominant oxidizer under diesel conditions.

References

1. Akihama, K., Takatori, Y., Inagaki, K., Sasaki, S. et al., "Mechanism of the Smokeless Rich Diesel Combustion by Reducing Temperature," SAE Technical Paper 2001-01-0655, 2001, doi:10.4271/2001-01-0655.
2. Gallo, Y., Simonsson, J., Lind, T., Bengtsson, P. et al., "A Study of In-Cylinder Soot Oxidation by Laser Extinction Measurements During an EGR-Sweep in an Optical Diesel Engine," SAE Technical Paper 2015-01-0800, 2015, doi:10.4271/2015-01-0800.

3. Gallo, Y., Li, Z., Richter, M., Andersson, Ö., "A Study of In-Cylinder Soot Oxidation by Laser Extinction Measurements During an EGR-Sweep in an Optical Diesel Engine," SAE Technical Paper 2016-01-2183, 2016, doi:10.4271/2016-01-2183.
4. Aronsson, U., Chartier, C., Andersson, Ö., Egnell, R. et al., "Analysis of the Correlation Between Engine-Out Particulates and Local Φ in the Lift-Off Region of a Heavy Duty Diesel Engine Using Raman Spectroscopy," SAE Technical Paper 2009-01-1357, 2009, doi:10.4271/2009-01-1357.
5. Dec, J. and Kelly-Zion, P., "The Effects of Injection Timing and Diluent Addition on Late-Combustion Soot Burnout in a DI Diesel Engine Based on Simultaneous 2-D Imaging of OH and Soot," SAE Technical Paper 2000-01-0238, 2000, doi:10.4271/2000-01-0238
6. Bartok, W., Sarofim, A.F., "Fossil Fuel Combustion: A Source Book " New York. Wiley; 1991.
7. Haynes, B.S., Wagner, H.Gg., "Soot formation", Progress in Energy and Combustion Science, 1981;7:229–273, http://dx.doi.org/10.1016/0360-1285(81)90001-0
8. Tree D.R., Svensson K.I., "Soot processes in compression ignition engines" Progress in Energy and Combustion Science Volume 33, Issue 3, June 2007, Pages 272–309, doi:10.1016/j.pecs.2006.03.002
9. Hayashida, K., Nagaoka, S., Ishitani, H., "Growth and oxidation of graphitic crystallites in soot particles within a laminar diffusion flame". In: Fuel 128 (2014), pp. 148-154. http://dx.doi.org/10.1016/j.fuel.2014.03.008
10. Guo, H., Anderson, P.M., Sunderland, P.B., "Optimized rate expressions for soot oxidation by OH and O2". In: Fuel 172 (2016), pp. 248-252. http://dx.doi.org/10.1016/j.fuel.2016.01.030

11. Bowditch, F., "A New Tool for Combustion Research A Quartz Piston Engine," SAE Technical Paper 610002, 1961, doi:10.4271/610002.
12. Hentschel, W. and Richter, J., "Time-Resolved Analysis of Soot Formation and Oxidation in a Direct-Injection Diesel Engine for Different EGR-Rates by an Extinction Method," SAE Technical Paper 952517, 1995, doi:10.4271/952517.
13. Tree, D. and Dec, J., "Extinction Measurements of In-Cylinder Soot Deposition in a Heavy-Duty DI Diesel Engine," SAE Technical Paper 2001-01-1296, 2001, doi:10.4271/2001-01-1296.
14. Mancaruso, E., Merola, S., and Vaglieco, B., "Soot Concentration and Particle Size in a DI CR Diesel Engine by Broadband Scattering and Extinction Measurements," SAE Technical Paper 2005-24-013, 2005, doi:10.4271/2005-24-013.
15. Xu, Y. and Lee, C., "Investigation of Soot Formation in Diesel Combustion Using Forward Illumination Light Extinction (FILE) Technique," SAE Technical Paper 2004-01-1411, 2004, doi:10.4271/2004-01-1411.
16. Cenker, E., Bruneaux, G., Pickett, L., and Schulz, C., "Study of Soot Formation and Oxidation in the Engine Combustion Network (ECN), Spray A: Effects of Ambient Temperature and Oxygen Concentration," *SAE Int. J. Engines* 6(1):352-365, 2013, doi:10.4271/2013-01-0901.
17. Manin, J., Pickett, L., and Skeen, S., "Two-Color Diffused Back-Illumination Imaging as a Diagnostic for Time-Resolved Soot Measurements in Reacting Sprays," *SAE Int. J. Engines* 6(4):1908-1921, 2013, doi:10.4271/2013-01-2548.
18. Bohren, C.F and D.R. Huffman, “Absorption and scattering of light by small particles”. 1998, New York, Wiley.
19. F. Migliorini, K. Thomson and G. Smallwood, “Investigation of optical properties of aging soot” Applied Physics B, 2011. 104(2): 273-283.

20. Shen, M., Malmborg, V., Gallo, Y., Waldheim, B. et al., "Analysis of Soot Particles in the Cylinder of a Heavy Duty Diesel Engine with High EGR," SAE Technical Paper 2015-24-2448, 2015, doi:10.4271/2015-24-2448.
21. Malmborg, V.B., Eriksson, A.C., Shen M., Nilsson, P. et al., "Evolution of in-cylinder diesel soot and emission characteristics investigated with on-line aerosol mass spectrometry", submitted to Journal of Environmental Science & Technology.
22. Onasch, T.B., Trimborn, A., Fortner, E.C., Jayne, J.T., et al., "Soot Particle Aerosol Mass Spectrometer: Development, Validation, and Initial Application", Aerosol Science and Technology, 2012, http://dx.doi.org/10.1080/02786826.2012.663948
23. Kamimoto, T. and Bae, M., "High Combustion Temperature for the Reduction of Particulate in Diesel Engines," SAE Technical Paper 880423, 1988, doi:10.4271/880423
24. LOGE AB. LOGEsoft. http://loge.se/Products/products.html. [accessed 04.09.2016].
25. Lars Seidel et al. "Comprehensive kinetic modeling and experimental study of a fuel-rich, premixed n-heptane flame". In: Combustion and Flame 162.5 (2015), pp. 2045 – 2058. http://dx.doi.org/10.1016/j.combustflame.2015
26. Wang, X., Song, C., Lu G., Song, J., et al., "Evolution of in-cylinder polycyclic aromatic hydrocarbons in a diesel engine fueled with n-heptane and n-heptane/toluene". In: Fuel 158 (2015), pp. 322-329. http://dx.doi.org/10.1016/j.fuel.2015.05.053
27. Machrafi, H., Cavadias, S., Gilbert, P., "An experimental and numerical analysis of the HCCI auto-ignition process of primary reference fuels, toluene reference fuels and diesel fuel in an engine, varying the engine parameters". In: Fuel 89 (2008), pp. 1007-1016. http://dx.doi.org/10.1016/j.fuproc.2008.03.007

28. Chen, W., Shuai, S., Wang, J., “A soot formation embedded reduced reaction mechanism for diesel surrogate fuel”. In: Fuel 88 (2009), pp. 1927-1936. http://dx.doi.org/10.1016/j.fuel.2009.03.039

29. Neoh, K.G., Howard, J.B., Sarofim A.F. (1974) Effect of oxidation on the physical structure of soot. Proc. Comb. Inst. 20:951